A kernel gradient free (KGF) SPH method

Article *in* International Journal for Numerical Methods in Fluids · March 2015

DOI: 10.1002/fld.4037

4 authors, including:

Can Huang
Peking University
23 PUBLICATIONS **106** CITATIONS
SEE PROFILE

Jia-Mei Lei
South China University of Technology
14 PUBLICATIONS **45** CITATIONS
SEE PROFILE

INTERNATIONAL JOURNAL FOR NUMERICAL METHODS IN FLUIDS
Int. J. Numer. Meth. Fluids 2015; **78**:691–707
Published online 21 April 2015 in Wiley Online Library (wileyonlinelibrary.com). DOI: 10.1002/fld.4037

A kernel gradient free (KGF) SPH method

C. Huang[1,*,†], J. M. Lei[1], M. B. Liu[2,3] and X. Y. Peng[1]

[1]*School of Aerospace Engineering, Beijing Institute of Technology, Beijing, 100081, China*
[2]*State Key Laboratory for Turbulence and Complex Systems, Peking University, Beijing, 100871, China*
[3]*College of Engineering, Peking University, Beijing, 100871, China*

SUMMARY

The finite particle method (FPM) is a modified SPH method with high order accuracy while retaining the advantages of SPH in modeling problems with free surfaces, moving interfaces, and large deformations. In both SPH and FPM, kernel gradient is necessary in kernel and particle approximation of a field function and its derivatives. In this paper, a new FPM is presented, which only involves kernel function itself in kernel and particle approximation. The kernel gradient is not necessary in the whole computation, and this approach is thus referred to as a kernel gradient free (KGF) SPH method. This is helpful when a kernel function is not differentiable or the resultant kernel gradient is not sufficiently smooth, and thus it is more general in selecting a kernel function. Moreover, different from the original FPM with an asymmetric corrective matrix, in the new FPM, the resultant corrective matrix is symmetric, and this is advantageous in particle approximations. A series of numerical examples have been conducted to show the efficiencies of KGF-SPH including one-dimensional mathematical tests of polynomial functions with equal or variable smoothing length and two-dimensional incompressible fluid flow of shear cavity. It is found that KGF-SPH is comparable with FPM in accuracy and is flexible as SPH. Copyright © 2015 John Wiley & Sons, Ltd.

Received 14 October 2014; Revised 17 February 2015; Accepted 24 March 2015

KEY WORDS: SPH; finite particle method (FPM); consistency; kernel function; kernel gradient

1. INTRODUCTION

SPH is a 'truly' mesh-free, particle method originally used for continuum scale applications and may be regarded as the oldest modern mesh-free particle method. In SPH, the state of a system is represented by a set of particles, which possess individual material properties and interact with each other within a certain range defined as a support domain by a weight function or smoothing function (or kernel function) [1]. Flow field variables (such as density, velocity, and acceleration) can be obtained through approximating the governing equations that are discretized on the set of particles. The SPH method was originally invented to solve astrophysical problems in the open space by Lucy [2] and Gingold and Monaghan [3], because the collective movement of those particles is similar to the movement of a liquid or gas flow, and it can be modeled by the governing equations of the classical Newtonian hydrodynamics. As a comparatively new computational method, SPH combines the advantages of mesh-free, Lagrangian, and particle methods. Particles are used to represent the state of a system, and these particles can freely move according to internal particle interactions and external forces. Therefore, it can naturally obtain history of fluid motion and can easily track material interfaces, free surfaces, and moving boundaries. The mesh-free nature of SPH method removes the difficulties caused by large deformations because SPH uses particles rather than mesh as a computational frame to approximate related governing equations. These features of SPH make it fairly attractive in

*Correspondence to: Can Huang, School of Aerospace Engineering, Beijing Institute of Technology, Beijing, 100081, China.
†E-mail: huangcancan@163.com

modeling complex flows with free surfaces, moving interfaces, and large deformations. Therefore, since its invention, the SPH method has been extensively studied and extended to different problems in engineering and sciences such as multi-phase flows [4, 5], multi-scale flows [6], high strain hydrodynamics with material strength [7–10], explosion and underwater explosion [11–13], and many others [14–16].

Despite its great success and wide applications, the conventional SPH method has been frustrated with some inherent numerical problems that motivate different modifications and corrections. One of the notorious problems of SPH is its low accuracy, which is originated from the particle inconsistency [14, 15]. The particle inconsistency problem in SPH results from the particle approximation process and is a manifestation of the discrepancy between the spatially discretized equations and the corresponding kernel approximations in a continuous form. To restore the particle consistency and improve the approximation accuracy, different approaches have been attempted. The symmetrization and anti-symmetrization in some SPH formulations [6, 16] make an actually early effort to try to restore particle consistency. Later approaches usually involve some kinds of normalization [5, 6, 11] or reconstruction of the smoothing function [15, 17, 18]. Based on Taylor series expansion on the SPH approximation of a function, Chen *et al.* [17] suggested a corrective smoothed particle method (CSPM). CSPM has better accuracy than the conventional SPH method as it solves the boundary deficiency problem. It was reported that the CSPM can also reduce the so-called tensile instability inherent in the traditional SPH method [18, 19]. Following similar ideas with Taylor series expansion, Liu *et al.* [20, 21] proposed a finite particle method (FPM), which uses a set of basis function to approximate field variables at a set of arbitrarily distributed particles. FPM can be regarded as an improved version of SPH and CSPM with better performance in particle consistency. Batra *et al.* [22] concurrently developed an idea similar to FPM, and it is named as modified SPH with applications mainly to solid mechanics problems. Fang *et al.* [23] further improved FPM for simulating free surface flows.

In the conventional SPH and the modified or corrected versions, both the kernel function and its gradients are used in the numerical approximations of a field function and its derivatives. These lead to some special requirements on the kernel function such as normalization condition, delta function behavior, and compact condition [1]. Also, the kernel gradient should exist (or the smoothing kernel function should be differentiable) and be sufficiently smooth. These requirements usually limit the selection of a kernel function. In this paper, a new FPM is presented, which only involves kernel function itself in kernel and particle approximation. The kernel gradient is not necessary in the whole computation, and this approach is thus referred to as a kernel gradient free (KGF) SPH method.

This paper is organized as follows. In Section 2, the conventional SPH, FPM, and KGF-SPH are briefly introduced, while their features are comparatively analyzed. In Section 3, the equations of motion for incompressible flows are described for the Navier–Stokes equations using KGF-SPH. In Section 4, KGF-SPH is mathematically analyzed for a number of one-dimensional polynomial functions with equal or variable smoothing lengths. In Section 5, KGF-SPH is applied to a two-dimensional lid-driven shear cavity problem. The paper ends in Section 6 with some further discussions.

2. METHODOLOGIES

2.1. The conventional SPH method

In the conventional SPH method, the kernel approximation of a field function $f(\boldsymbol{r})$ at a certain particle located at position $\boldsymbol{r}$ is [16]

$$f(\mathbf{r}) = \int f(\mathbf{r}')W dV, \tag{1}$$

where W is the smoothing function (or kernel function or even simply abbreviated as kernel), $\boldsymbol{r}'$ is the neighboring particle of the particle $\boldsymbol{r}$, and dV is the volume element of the particle $\boldsymbol{r}'$.

The SPH kernel approximation of a spatial derivative is

$$\nabla f_{\mathbf{r}}(\mathbf{r}) = \int f(\mathbf{r}')\nabla_{\mathbf{r}} W dV, \tag{2}$$

DOI: 10.1002/fld

where $\nabla_r W$ is the gradient of the smoothing function W. Eqns (1) and (2) have C^1 kernel consistency for the interior regions. However, for the boundary regions, it even does not have C^0 kernel consistency [20]. By using a symmetrization process, Eq. (2) can be rewritten as

$$\nabla_{\mathbf{r}} f(\mathbf{r}) = \int \left[f\left(\mathbf{r}'\right) - f(\mathbf{r}) \right] \nabla_{\mathbf{r}} W dV. \tag{3}$$

Eq. (3) actually uses the particle inconsistency in approximating the derivative of the smoothing function to offset or balance the particle inconsistency in approximating the derivatives of a function and thus to improve the accuracy of the approximations [20].

2.2. Finite particle method

Using Taylor series expansion of a function in a three-dimensional space and neglecting the second and high order derivatives, we can obtain

$$f\left(\mathbf{r}'\right) = f(\mathbf{r}) + \nabla f(\mathbf{r}) \cdot \left(\mathbf{r}' - \mathbf{r}\right) + o\left(h^2\right). \tag{4}$$

Multiplying both sides of Eq. (4) with a smoothing function W and its first order derivatives ∇W and integrating the resulting equation over the computational domain, the following equations [21] are derived

$$\int f\left(\mathbf{r}'\right) W dV = f(\mathbf{r}) \int W dV + \nabla f(\mathbf{r}) \cdot \int \left(\mathbf{r}' - \mathbf{r}\right) W dV, \tag{5}$$

$$\int f\left(\mathbf{r}'\right) \nabla W dV = f(\mathbf{r}) \int \nabla W dV + \nabla f(\mathbf{r}) \cdot \int \left(\mathbf{r}' - \mathbf{r}\right) \nabla W dV. \tag{6}$$

For convenience, f, ∇f, and f' are used to represent $f(\boldsymbol{r})$, $\nabla f(\boldsymbol{r})$, and $f(\boldsymbol{r}')$ in the following, respectively. Solving Eqns (5) and (6) together, we have

$$\begin{bmatrix} f \\ \nabla f \end{bmatrix} = \boldsymbol{A} \begin{bmatrix} \int f' W dV \\ \int f' \nabla W dV \end{bmatrix}, \tag{7}$$

where the corrective matrix $\boldsymbol{A}$ is expressed as follows:

$$\boldsymbol{A} = \begin{bmatrix} \int W dV & \int \left(x' - x\right) W dV & \int \left(y' - y\right) W dV & \int \left(z' - z\right) W dV \\ \int W_x dV & \int \left(x' - x\right) W_x dV & \int \left(y' - y\right) W_x dV & \int \left(z' - z\right) W_x dV \\ \int W_y dV & \int \left(x' - x\right) W_y dV & \int \left(y' - y\right) W_y dV & \int \left(z' - z\right) W_y dV \\ \int W_z dV & \int \left(x' - x\right) W_z dV & \int \left(y' - y\right) W_z dV & \int \left(z' - z\right) W_z dV \end{bmatrix}^{-1}, \tag{8}$$

where x, y, and z are the three components of the position vector $\boldsymbol{r}$. Similarly, x', y', and z' are the three components of the position vector $\boldsymbol{r}'$.

Compared with CSPM [17–19, 24], Eq. (7) calculates simultaneously a function and all its derivatives, and except for the function values, no lower order derivatives are inherent in approximating the higher order derivatives. Therefore, the possible numerical errors existed in a lower order derivative will not be brought to the higher order derivatives. Eq. (7) has first order kernel consistency for both the interior and boundary regions if only the first order derivatives are retained in the Taylor series expansion. If discretizing Eq. (7) with particle approximation, it is further demonstrated that the corresponding particle approximation also has first order particle consistency for both the interior and boundary particles [20].

DOI: 10.1002/fld

Moreover, from Eqns (2) and (7), it is observed that the kernel gradients ($\nabla_{\boldsymbol{r}} W$) are used in numerical approximation of the gradients of a field function in SPH, and they are also used in numerical approximation of both the field function and its gradients in FPM. For such purposes, the kernel gradients should exist (or the smoothing kernel function should be differentiable) and be sufficiently smooth. These requirements usually limit the selection of a kernel function.

2.3. Kernel gradient free SPH – a modified finite particle method

If using $(\boldsymbol{r}' - \boldsymbol{r})W$ instead of ∇W in Eq. (6), then the expression of Eq. (6) changes as

$$\int f(\mathbf{r}')(\mathbf{r}' - \mathbf{r}) W dV = f(\mathbf{r}) \int (\mathbf{r}' - \mathbf{r}) W dV + \nabla f(\mathbf{r}) \cdot \int (\mathbf{r}' - \mathbf{r})^2 W dV + o(h^2). \tag{9}$$

Solving Eqns (5) and (9) simultaneously, we have

$$\begin{bmatrix} f \\ \nabla f \end{bmatrix} = \boldsymbol{A}^* \begin{bmatrix} \int f' W dV \\ \int f' (\mathbf{r}' - \mathbf{r}) W dV \end{bmatrix}, \tag{10}$$

where

$$\mathbf{A}^* = \begin{bmatrix} \int W dV & \int (x' - x) W dV & \int (y' - y) W dV & \int (z' - z) W dV \\ \int (x' - x) W dV & \int (x' - x)(x' - x) W dV & \int (x' - x)(y' - y) W dV & \int (x' - x)(z' - z) W dV \\ \int (y' - y) W dV & \int (y' - y)(x' - x) W dV & \int (y' - y)(y' - y) W dV & \int (y' - y)(z' - z) W dV \\ \int (z' - z) W dV & \int (z' - z)(x' - x) W dV & \int (z' - z)(y' - y) W dV & \int (z' - z)(z' - z) W dV \end{bmatrix}^{-1}. \tag{11}$$

The KGF-SPH has three advantages:

1. No matter whether the kernel gradients exist or not, the numerical approximation can proceed. This is different from the conventional SPH and FPM in which the kernel gradient should exist so as to proceed approximations for a field function and its gradient. This greatly widens the selection of the kernel function.
2. From Eq. (11), as KGF-SPH is a truly kernel gradient free SPH method, it is seen that the corrective matrix $\boldsymbol{A}^*$ in KGF-SPH is invertible. However, the corrective matrix $\boldsymbol{A}$ in FPM may not be invertible especially when the kernel gradients do not exist or equal to zero.
3. The corrective matrix $\boldsymbol{A}^*$ has a good symmetry, and the symmetric properties of the matrix can simplify the solving progress and can save the computational time.

In this paper, we adopt the widely used cubic spline function [14, 25] as the smoothing function:

$$W(R,h) = \alpha_d \begin{cases} \frac{2}{3} - R^2 + \frac{1}{2}R^3 & 0 \le R < 1 \\ \frac{1}{6}(2-R)^3 & 1 \le R < 2 \\ 0 & 2 \le R \end{cases}, \tag{12}$$

where $R = |\boldsymbol{r} - \boldsymbol{r}'| / h$ and α_d is $1/h$ and $15/(7\pi h^2)$ in one-dimensional and two-dimensional spaces, respectively. Figure 1 shows the distribution of the cubic spline kernel function in one-dimensional and two-dimensional spaces.

DOI: 10.1002/fld

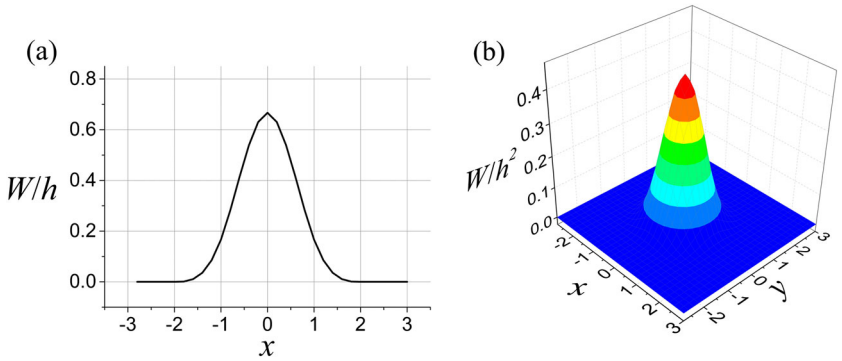

Figure 1. Illustration of the cubic spline kernel function in (a) one-dimensional and (b) two-dimensional spaces.

3. EQUATIONS OF MOTION FOR FLUID FLOW

3.1. Governing equations for incompressible flows

For incompressible flows, assuming the dissipation coefficient μ is a constant, the continuity and momentum equations in a Lagrangian frame are

$$\frac{d\rho}{dt} = -\rho\nabla\cdot\mathbf{V}, \tag{13}$$

$$\frac{dv_\alpha}{dt} = -\frac{1}{\rho}\frac{\partial p}{\partial x_\alpha} + \frac{1}{\rho}\mu\frac{\partial \varepsilon_{\alpha\beta}}{\partial x_\beta}, \tag{14}$$

where t represents time, ρ is the scalar density, $\boldsymbol{V}$ is the velocity vector, v_α represents the velocity component, x_α and x_β are the spatial coordinates, $\delta_{\alpha\beta}$ is the Dirac symbol, and $\varepsilon_{\alpha\beta}$ represents the strain rate component, expressed as:

$$\varepsilon_{\alpha\beta} = \frac{\partial v_\alpha}{\partial x_\beta} + \frac{\partial v_\beta}{\partial x_\alpha} - \frac{2}{3}\nabla\cdot\mathbf{V}\delta_{\alpha\beta}. \tag{15}$$

3.2. Equations of motion in discretized form

In the two-dimensional space, by using KGF-SPH method, the continuity Eq. (13) is discretized as

$$\frac{d\rho_i}{dt} = -\rho_i \begin{pmatrix} \boldsymbol{A}^*_{21}\sum_j v_{x,j} W\frac{m_j}{\rho_j} + \boldsymbol{A}^*_{22}\sum_j v_{x,j}(x_j - x_i) W\frac{m_j}{\rho_j} + \boldsymbol{A}^*_{23}\sum_j v_{x,j}(y_j - y_i) W\frac{m_j}{\rho_j} \\ +\boldsymbol{A}^*_{31}\sum_j v_{y,j} W\frac{m_j}{\rho_j} + \boldsymbol{A}^*_{32}\sum_j v_{y,j}(x_j - x_i) W\frac{m_j}{\rho_j} + \boldsymbol{A}^*_{33}\sum_j v_{y,j}(y_j - y_i) W\frac{m_j}{\rho_j} \end{pmatrix}, \tag{16}$$

where i and j denote the particle i and particle j, respectively, A^*_{mn} represents the component of the corrective matrix $\boldsymbol{A}^*$, m_i and m_j, and ρ_i and ρ_j are the mass and density of particle i and particle j, respectively, and $v_{x,j}$ and $v_{y,j}$ are the velocity components of particle j in x direction and y direction, respectively.

DOI: 10.1002/fld

The discretized momentum equations in x and y directions are respectively

$$\begin{aligned}\frac{dv_{xi}}{dt} = &-\frac{1}{\rho_i}\left(\mathbf{A}^*_{21}\sum_j p_j W\frac{m_j}{\rho_j} + \mathbf{A}^*_{22}\sum_j p_j\left(x_j - x_i\right)W\frac{m_j}{\rho_j} + \mathbf{A}^*_{23}\sum_j p_j\left(y_j - y_i\right)W\frac{m_j}{\rho_j}\right)\\ &+\frac{\mu}{\rho_i}\left(\mathbf{A}^*_{21}\sum_j \varepsilon_{xx,j} W\frac{m_j}{\rho_j} + \mathbf{A}^*_{22}\sum_j \varepsilon_{xx,j}\left(x_j - x_i\right)W\frac{m_j}{\rho_j} + \mathbf{A}^*_{23}\sum_j \varepsilon_{xx,j}\left(y_j - y_i\right)W\frac{m_j}{\rho_j}\right)\\ &+\frac{\mu}{\rho_i}\left(\mathbf{A}^*_{31}\sum_j \varepsilon_{xy,j} W\frac{m_j}{\rho_j} + \mathbf{A}^*_{32}\sum_j \varepsilon_{xy,j}\left(x_j - x_i\right)W\frac{m_j}{\rho_j} + \mathbf{A}^*_{33}\sum_j \varepsilon_{xy,j}\left(y_j - y_i\right)W\frac{m_j}{\rho_j}\right),\end{aligned} \tag{17}$$

$$\begin{aligned}\frac{dv_{yi}}{dt} = &-\frac{1}{\rho_i}\left(\mathbf{A}^*_{31}\sum_j p_j W\frac{m_j}{\rho_j} + \mathbf{A}^*_{32}\sum_j p_j\left(x_j - x_i\right)W\frac{m_j}{\rho_j} + \mathbf{A}^*_{33}\sum_j p_j\left(y_j - y_i\right)W\frac{m_j}{\rho_j}\right)\\ &+\frac{\mu}{\rho_i}\left(\mathbf{A}^*_{21}\sum_j \varepsilon_{xy,j} W\frac{m_j}{\rho_j} + \mathbf{A}^*_{22}\sum_j \varepsilon_{xy,j}\left(x_j - x_i\right)W\frac{m_j}{\rho_j} + \mathbf{A}^*_{23}\sum_j \varepsilon_{xy,j}\left(y_j - y_i\right)W\frac{m_j}{\rho_j}\right)\\ &+\frac{\mu}{\rho_i}\left(\mathbf{A}^*_{31}\sum_j \varepsilon_{yy,j} W\frac{m_j}{\rho_j} + \mathbf{A}^*_{32}\sum_j \varepsilon_{yy,j}\left(x_j - x_i\right)W\frac{m_j}{\rho_j} + \mathbf{A}^*_{33}\sum_j \varepsilon_{yy,j}\left(y_j - y_i\right)W\frac{m_j}{\rho_j}\right),\end{aligned} \tag{18}$$

where p_j is the pressure of particle j and $\varepsilon_{\alpha\beta,j}$ represents the strain rate component of particle j. And the discretization of the corrective matrix $\boldsymbol{A}^*$ is

$$\mathbf{A}^* = \begin{bmatrix} \sum W\frac{m_j}{\rho_j} & \sum x_{ji} W\frac{m_j}{\rho_j} & \sum y_{ji} W\frac{m_j}{\rho_j} \\ \sum x_{ji} W\frac{m_j}{\rho_j} & \sum x_{ji}^2 W\frac{m_j}{\rho_j} & \sum x_{ji} y_{ji} W\frac{m_j}{\rho_j} \\ \sum y_{ji} W\frac{m_j}{\rho_j} & \sum x_{ji} y_{ji} W\frac{m_j}{\rho_j} & \sum y_{ji}^2 W\frac{m_j}{\rho_j} \end{bmatrix}^{-1}. \tag{19}$$

where $x_{ji}=x_j-x_i$, $y_{ji}=y_j-y_i$. Similarly, we can get the discrete forms of the strain rate components $\varepsilon_{xx,i}$, $\varepsilon_{xy,i}$, and $\varepsilon_{yy,i}$, which are expressed as the following forms respectively:

$$\begin{aligned}\varepsilon_{xxi} = &2\left(\mathbf{A}^*_{21}\sum_j v_{x,j} W\frac{m_j}{\rho_j} + \mathbf{A}^*_{22}\sum_j v_{x,j}\left(x_j - x_i\right)W\frac{m_j}{\rho_j} + \mathbf{A}^*_{23}\sum_j v_{x,j}\left(y_j - y_i\right)W\frac{m_j}{\rho_j}\right)\\ &-\frac{2}{3}\left(\mathbf{A}^*_{21}\sum_j v_{x,j} W\frac{m_j}{\rho_j} + \mathbf{A}^*_{22}\sum_j v_{x,j}\left(x_j - x_i\right)W\frac{m_j}{\rho_j} + \mathbf{A}^*_{23}\sum_j v_{x,j}\left(y_j - y_i\right)W\frac{m_j}{\rho_j}\right)\\ &-\frac{2}{3}\left(\mathbf{A}^*_{31}\sum_j v_{y,j} W\frac{m_j}{\rho_j} + \mathbf{A}^*_{32}\sum_j v_{y,j}\left(x_j - x_i\right)W\frac{m_j}{\rho_j} + \mathbf{A}^*_{33}\sum_j v_{y,j}\left(y_j - y_i\right)W\frac{m_j}{\rho_j}\right),\end{aligned} \tag{20}$$

$$\begin{aligned}\varepsilon_{xyi} = &\left(\mathbf{A}^*_{21}\sum_j v_{y,j} W\frac{m_j}{\rho_j} + \mathbf{A}^*_{22}\sum_j v_{y,j}\left(x_j - x_i\right)W\frac{m_j}{\rho_j} + \mathbf{A}^*_{23}\sum_j v_{y,j}\left(y_j - y_i\right)W\frac{m_j}{\rho_j}\right)\\ &-\left(\mathbf{A}^*_{31}\sum_j v_{x,j} W\frac{m_j}{\rho_j} + \mathbf{A}^*_{32}\sum_j v_{x,j}\left(x_j - x_i\right)W\frac{m_j}{\rho_j} + \mathbf{A}^*_{33}\sum_j v_{x,j}\left(y_j - y_i\right)W\frac{m_j}{\rho_j}\right),\end{aligned} \tag{21}$$

DOI: 10.1002/fld

$$\begin{aligned}\varepsilon_{yyi} = 2&\left(\mathbf{A}^*_{31}\sum_j v_{y,j}W\frac{m_j}{\rho_j} + \mathbf{A}^*_{32}\sum_j v_{y,j}(x_j - x_i)W\frac{m_j}{\rho_j} + \mathbf{A}^*_{33}\sum_j v_{y,j}(y_j - y_i)W\frac{m_j}{\rho_j}\right)\\ -\frac{2}{3}&\left(\mathbf{A}^*_{21}\sum_j v_{x,j}W\frac{m_j}{\rho_j} + \mathbf{A}^*_{22}\sum_j v_{x,j}(x_j - x_i)W\frac{m_j}{\rho_j} + \mathbf{A}^*_{23}\sum_j v_{x,j}(y_j - y_i)W\frac{m_j}{\rho_j}\right)\\ -\frac{2}{3}&\left(\mathbf{A}^*_{31}\sum_j v_{y,j}W\frac{m_j}{\rho_j} + \mathbf{A}^*_{32}\sum_j v_{y,j}(x_j - x_i)W\frac{m_j}{\rho_j} + \mathbf{A}^*_{33}\sum_j v_{y,j}(y_j - y_i)W\frac{m_j}{\rho_j}\right).\end{aligned} \tag{22}$$

3.3. Artificial equation of state for modeling incompressible flows

In this paper, pressure is solved by using the weakly compressible equation [26], which is expressed as

$$p = c^2(\rho - \rho_\infty), \tag{23}$$

where ρ_∞ is the reference density and c is the artificial sound speed, which is usually taken as $10\,V_{max}$ in the SPH method. In order to meet the incompressible properties better, the artificial sound speed is taken as $50\,V_{max}$ in this paper.

For time discretization scheme, the leapfrog method is used in this paper, and readers may refer to the work of Liu *et al.* [27] for more details. The principle of selecting timestep is $dt < CFL\frac{h}{c+V_{max}}$, where $CFL = 0.1$ in this paper.

4. NUMERICAL ANALYSES

In this section, numerical analyses are conducted in testing the KGF-SPH for a number of polynomials as the reproducibility of polynomials actually reflect the accuracy of kernel and particle approximations (e.g., kernel and particle consistency). Cases with equal and variable smoothing length are taken to show the performance of KGF-SPH for modeling problems with regularly and irregularly distributed particles. Also, for the sake of comparison, numerical results obtained with SPH, FPM, and KGF-SPH are all provided.

4.1. Linear function $f = x$

In this example, a linear function $f = x$ is considered in one-dimensional domain of $[-0.5, 0.5]$ to examine the accuracy of KGF-SPH. Depending on whether the particles are uniformly distributed or not, the following discussion are divided into two cases: (1) uniformly distributed particles and (2) non-uniformly distributed particles.

4.1.1. Uniformly distributed particles. Particle distributions are shown in Figure 2, and there are two kinds of particles: inner particles and boundary particles. Particles are evenly distributed; the particle spacing is $\Delta = 0.1$, and the smoothing length is $h = 1.2\Delta$. The numerical results of the linear function and its first and second derivatives computed by SPH and KGF-SPH method are compared with the analytical solutions in Figure 3. From Figure 3, the results obtained by the SPH method exist large errors, while the results obtained by the KGF-SPH method are consistent with the

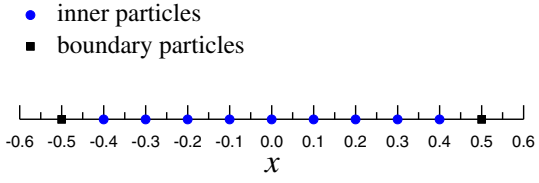

Figure 2. Schematic diagram of uniformly distributed particles.

DOI: 10.1002/fld

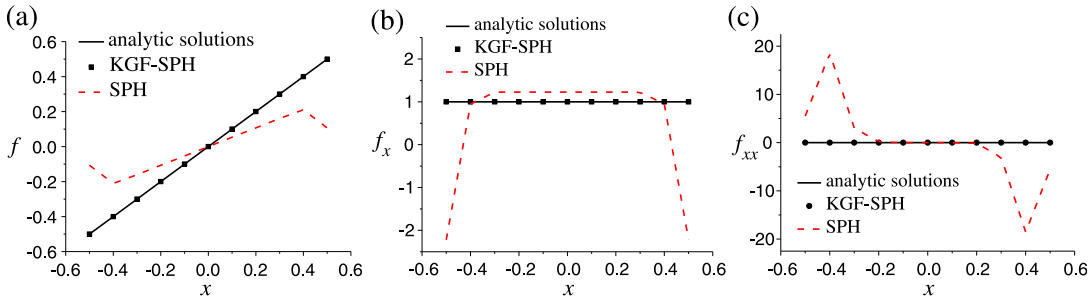

Figure 3. For the uniformly distributed particle, numerical results obtained by SPH and kernel gradient free (KGF) SPH are compared with the analytical solutions: (a) linear function, (b) first order derivative, and (c) second order derivative.

analytical solutions very well. It is clear that the KGF-SPH method improves the precision of the SPH method and has the capability of accurately reproducing a linear function and its derivatives. These conclusions agree with the conclusions using the original FPM [20].

4.1.2. Non-uniformly distributed particles. Figure 4 shows the inner and boundary particles distribution when particles are distributed non-uniformly. The particles' location and the smooth length are given by the following formulas:

$$x_i = x_{min} + \Delta_{min} \frac{1 - q^i}{1 - q}, \tag{24}$$

$$h_i = \varepsilon \Delta_{min} q^i, \tag{25}$$

where $x_{\min}$ is the minimum value in the X direction, $\Delta_{\min}$ is the minimum particle spacing, $\varepsilon = 1.2$ and q is set as 1.1 in this case. In Figures 5 and 6, the numerical results of the linear function and its first and second derivatives computed by SPH and KGF-SPH with the cubic and quintic splines [14] respectively are compared with the analytical solutions.

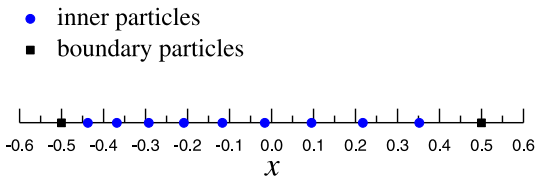

Figure 4. Schematic diagram of the non-uniformly distributed particles.

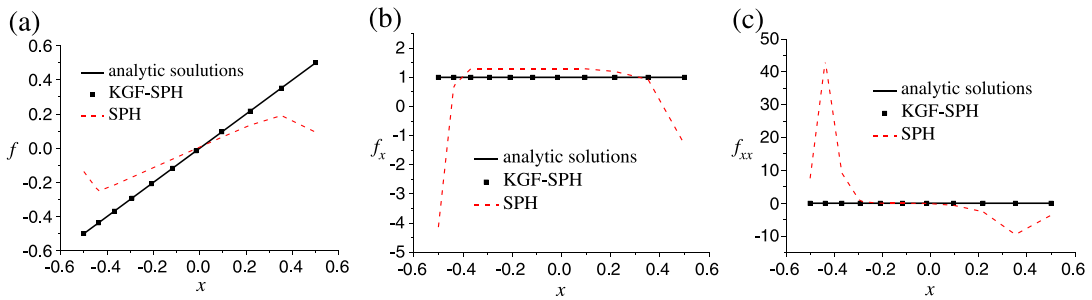

Figure 5. For the non-uniform distributed particles, numerical results obtained by SPH and kernel gradient free (KGF) SPH with the cubic spline are compared with the analytical solutions: (a) linear function, (b) first order derivative, and (c) second order derivative.

DOI: 10.1002/fld

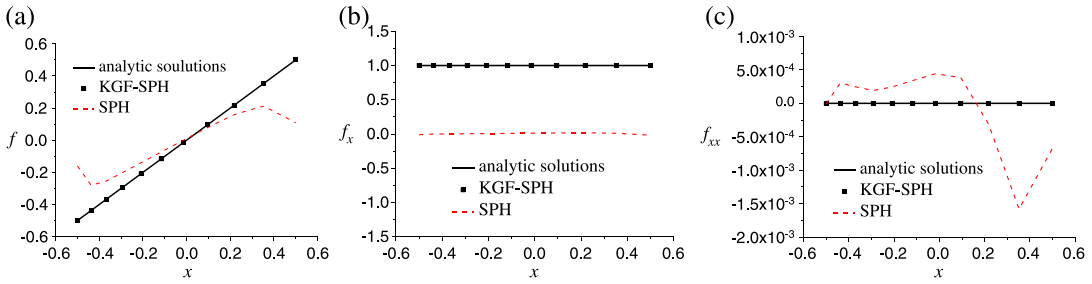

Figure 6. For the non-uniform distributed particles, numerical results obtained by SPH and kernel gradient free (KGF) SPH with the quintic spline are compared with the analytical solutions: (a) linear function, (b) first order derivative, and (c) second order derivative.

It is well known that the conventional SPH method is sensitive to the selection of kernel functions. Comparing Figure 5 with Figure 6, it is found that the results obtained by SPH with the quintic spline are superior to these obtained by SPH with the cubic spline. However, it is known that changing smoothing functions does not restore particle inconsistency of SPH method. Therefore, it is shown in Figures 5 and 6 that the conventional SPH method with the quintic and cubic splines both produce big errors. However, in Figures 5 and 6, it is seen that even for a non-uniform particle distribution, the KGF-SPH method with the quintic and cubic splines is both able to reproduce the linear function and its derivatives accurately. These suggest that KGF-SPH is not sensitive to the selection of smoothing functions and is able to reproduce a linear function and its derivatives accurately for even non-uniform distributed particles, but the conventional SPH method with the cubic and quintic splines has big errors. This conclusion is similar to what in the original FPM method [20], which is not sensitive to kernel selection and particle distribution.

4.2. *One-dimensional function* $f=x^5$

In the following example, we will examine the accuracy of this method through a one-dimensional function $f=x^5$, in which the range of x is $[-0.5, 0.5]$. We will only give the results of a uniformly distributed particle because the results of non-uniformly distributed particles are greatly similar to those of uniformly distributed particles. The following discussion is divided into two cases: (1) comparing SPH method, FPM, and KGF-SPH and (2) comparing different kernel functions, which are the cubic spline kernel function and the constant ($W=1$), respectively.

4.2.1. Comparing SPH method, finite particle method, and kernel gradient free SPH. The particle distribution is similar to that in Figure 2, where the particle spacing is $\Delta=0.05$ and the smoothing length is $h=1.2\Delta$. Figure 7 presents the results of SPH, FPM, and KGF-SPH compared with the analytical solutions. As can be seen from the figure, the results of FPM and KGF-SPH are close to the analytical solutions and more accurate than the results obtained by the SPH method. So both FPM and KGF-SPH have a higher precision than the SPH method when it comes to solving high

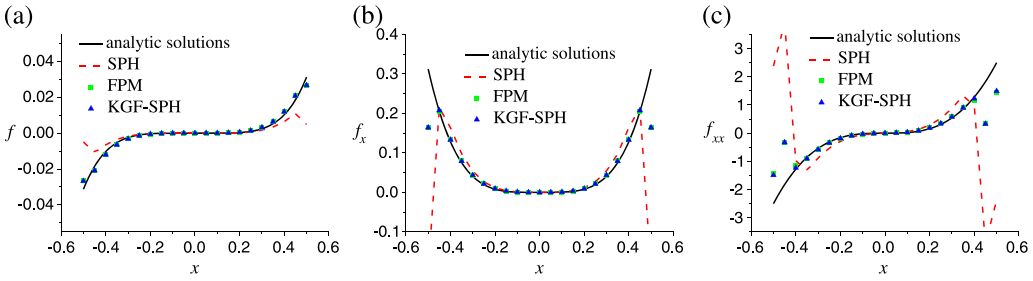

Figure 7. For uniformly distributed particles and the particle spacing $\Delta=0.05$, numerical results obtained by SPH, finite particle method (FPM) and kernel gradient free (KGF) SPH are compared with the analytical solutions: (a) field function, (b) first order derivative, and (c) second order derivative.

DOI: 10.1002/fld

order polynomial functions. The performance of KGF-SPH in modeling high order polynomials is as good as modeling the linear function.

In order to present the difference between FPM and KGF-SPH more clearly, we analyze the change rule of the numerical errors with the increase of the particle spacing. The numerical errors of the field function and its first and second derivatives are calculated by Eqns (26), (27), and (28), respectively. Figure 8 shows the numerical errors produced by FPM and KGF-SPH with changing particle spacing. As shown in Figure 8(a), the numerical errors of inner particles' field function produced by FPM are consistent with that produced by KGF-SPH. However, from Figure 8(b) and (c), we can see that numerical errors of inner particles' first and second derivatives produced by the KGF-SPH are smaller than those produced by FPM, and the differences between the two methods are more and more evident with the increase of the particle spacing. Therefore, we can conclude that the KGF-SPH method can further improve the approximation accuracy of the derivatives, compared with FPM.

$$e(f) = \frac{(f_{\text{FPM}} - f_{\text{exact solution}})_{max}}{(f_{max} - f_{min})}, \tag{26}$$

$$e(f_x) = \frac{(f_{x,\text{FPM}} - f_{x,\text{exact solution}})_{max}}{(f_{x,max} - f_{x,min})}, \tag{27}$$

$$e(f_{xx}) = \frac{(f_{xx,\text{FPM}} - f_{xx,exact\ solution})_{max}}{(f_{xx,max} - f_{xx,min})}. \tag{28}$$

4.2.2. Comparing different kernel functions. The particle distribution is shown in Figure 2, the particle spacing is $\Delta = 0.02$, and the smoothing length is $h = 1.2\Delta$. In Figure 9, the numerical solutions obtained by KGF-SPH with the cubic spline kernel function and the constant kernel function ($W = 1$) are compared with the analytical solutions. As seen from Figure 9(a), the numerical solutions of the field function for the two different kinds of kernel function agree well with the analytical solutions; as shown in Figure 9(b) and (c), the numerical solutions of the first and second derivatives for the two different kinds of kernel function are the same except for the solutions near the boundary. However, when the kernel function is the constant function ($W = 1$), the corrective matrix $\boldsymbol{A}$ in FPM is not reversible, so compared with FPM, KGF-SPH does not need the kernel function gradient and is more flexible and robust.

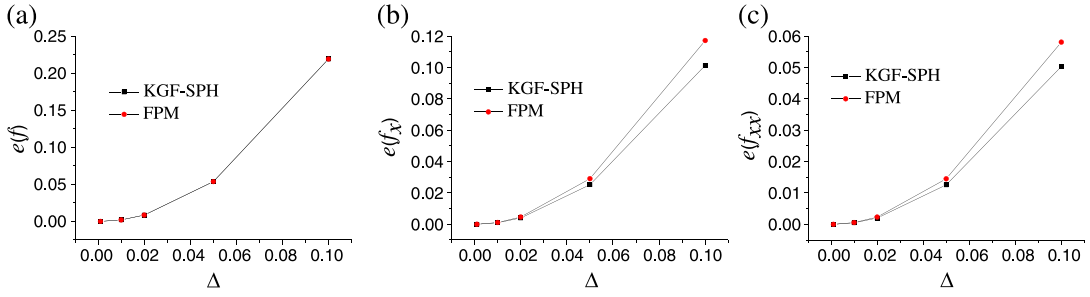

Figure 8. For uniformly distributed particles, numerical errors of inner particles' field function and derivatives produced by kernel gradient free (KGF) SPH are compared with that produced by finite particle method (FPM): (a) numerical errors of the field function, (b) numerical errors of first order derivative, and (c) numerical errors of second order derivative.

DOI: 10.1002/fld

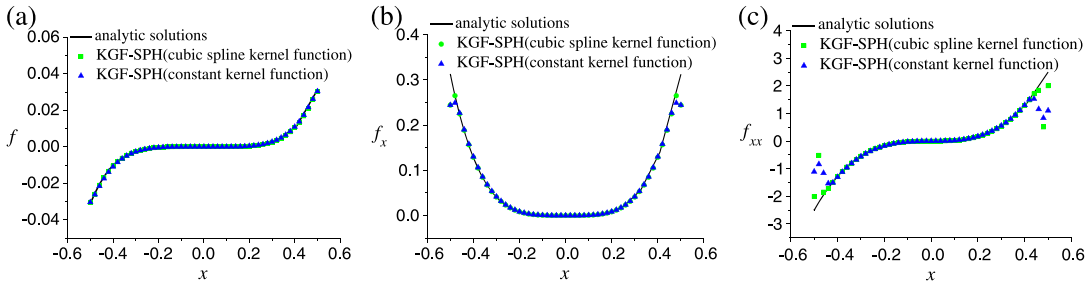

Figure 9. For uniformly distributed particles and the particle spacing $\Delta = 0.02$, when adopting different kernel functions, numerical solutions obtained by kernel gradient free (KGF) SPH are compared with the analytical solutions: (a) field function, (b) first order derivative, and (c) second order derivative.

5. KERNEL GRADIENT FREE SPH SIMULATION OF LID-DRIVEN SHEAR CAVITY

5.1. Geometric model and boundary conditions

The classic lid-driven shear cavity problem is the flow within a closed square generated by horizontally moving the top side of the square at a constant velocity $\boldsymbol{V}_\infty$, while the other three sides remain stationary. The problem geometry is shown in Figure 10. In order to improve the stability, particle-shifting technology [28, 29] is adopted in the calculation progress. Figure 11 is the particle distribution of a two-dimensional lid-driven shear cavity, and for the convenience of explanation, there are four kinds

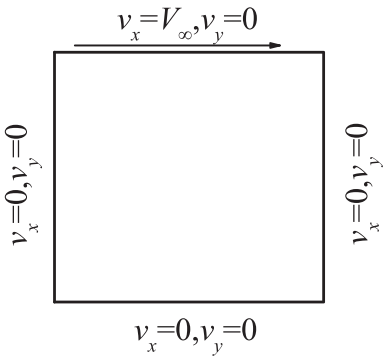

Figure 10. Schematic diagram of the lid-driven shear cavity.

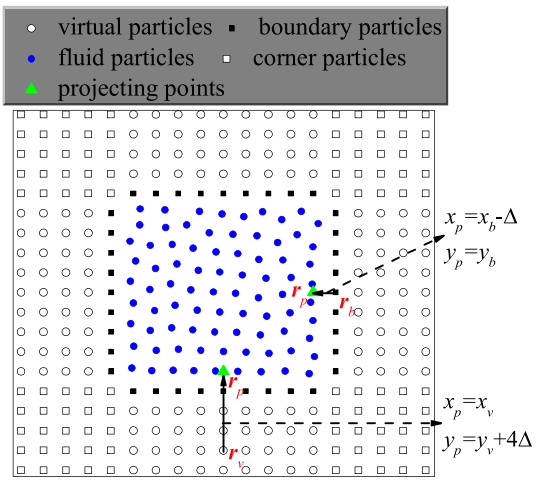

Figure 11. Schematic diagram of the particle distribution of the lid-driven shear cavity.

DOI: 10.1002/fld

of particles in Figure 11, which are fluid particles, boundary particles, corner particles, and virtual particles, respectively. Herein, the subscripts f, b, c, and v are used to represent the fluid particles, boundary particles, corner particles, and virtual particles, respectively. In order to improve the accuracy of the results, we have four layers of virtual particles out of the boundary, as shown in Figure 11.

As shown in Figure 11, if a boundary particle (or the virtual particle) extends an increment $\eta\Delta$ into the flow field along the normal direction of the boundary particle (or the virtual particle), we can get a new point $\boldsymbol{r}_p$ corresponding with the boundary particle (or the virtual particle). The new inner point near the boundary is defined as the projecting point in this paper, using the subscript p to denote the projecting point. The displacement between boundary particles (or virtual particles) and projecting points satisfies the following relation:

$$\mathbf{r}_p = \mathbf{r}_b(\text{or } \mathbf{r}_v) + \boldsymbol{n}\eta\Delta, \tag{29}$$

where $\boldsymbol{r}_p$, $\boldsymbol{r}_b$, and $\boldsymbol{r}_v$ denote the coordinates of the projecting point, boundary particles, and virtual particles, respectively, $\boldsymbol{n}$ is the normal direction of boundary particles (or virtual particles), η is an adjustable parameter, and Δ is the initial particle spacing. In this paper, the principle of selecting η value should satisfy that the distance of projecting points to the boundary is Δ. The flow variables of projecting points are calculated by the following equation:

$$f_p = \frac{\sum_j \frac{m_j}{\rho_j} f_j W_{pj}}{\sum_j \frac{m_j}{\rho_j} W_{pj}}, \tag{30}$$

where f_p and f_j represent flow variables of projecting points and fluid particles, respectively. It should be noted that j only represents the fluid particles interacting with projecting points but does not contain boundary particles and virtual particles, as shown in Figure 12.

Based on the flow information of projecting points, the calculating approaches of flow variables of boundary particles, virtual particles, and corner particles will be given in the following.

1. Boundary particles: For the no slip and no penetration condition, the velocity of fluid particles on the wall should be zero. According to Prandtl's boundary layer theory, the pressure of boundary particles should satisfy $\partial p_b/\partial n_b = 0$ approximately, then according to Eq. (23), the density of boundary particles should satisfy $\partial \rho_b/\partial n_b = 0$ approximately. Therefore, the velocity and density of the boundary particles should be

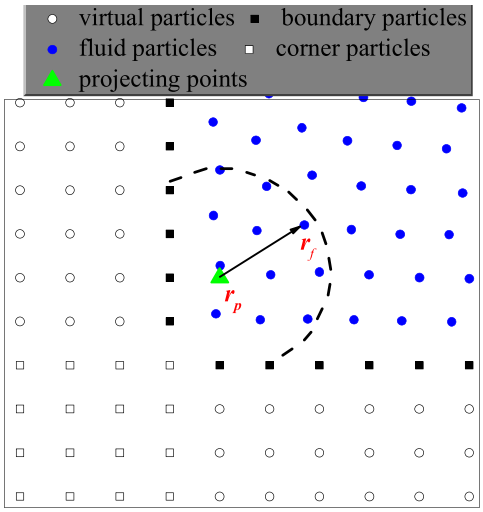

Figure 12. The fluid particles interacting with the projecting points.

DOI: 10.1002/fld

$$\begin{aligned} v_{x,b} &= 0, \\ v_{y,b} &= 0, \\ \rho_b &= \rho_p. \end{aligned} \tag{31}$$

2. Virtual particles: In the SPH method, there is a mirroring particle method [26, 30] in which virtual particles are generated by mirroring or reflecting fluid particles along solid boundaries. The velocities of the virtual particles are obtained through the ratios of the distances from fluid particles and virtual particles to the boundary. The original purpose of the mirroring particle method is to avoid fluid particles penetrating solid walls. In 2011, Fabricio *et al*. [31] tested the accuracy of mirroring particle method by the Poiseuille flow problem, and the results demonstrate that this method has higher accuracy.

The method used in this paper is similar to the mirroring particle method with a slight difference. It is well known that in boundary layer, the viscosity cannot be ignored; therefore, the velocity gradient of fluid particles in the boundary layer is important for the accuracy of the numerical results. Taking the right boundary of the cavity as examples, as shown in Figure 13, in order to ensure that the normal gradient of tangential velocity between virtual particles and the corresponding projecting points is equal to that between boundary particles and the corresponding projecting points, the following relationship should be satisfied:

$$\frac{v_{y,v} - v_{y,p}}{x_v - x_p} = \frac{v_{y,b} - v_{y,p}}{x_b - x_p}. \tag{32}$$

Compared with the normal gradient of tangential velocity, the other velocity gradients are not important and are hence ignored for convenience in this paper. Therefore, flow variables of virtual particles out of the right boundary can be calculated by the following formulas:

$$\begin{aligned} v_{x,v} &= 0, \\ v_{y,v} &= v_{y,p} + \frac{x_v - x_p}{x_b - x_p}\left(v_{y,b} - v_{y,p}\right), \\ \rho_v &= \rho_p. \end{aligned} \tag{33}$$

Similarly, flow variables of virtual particles out of the other boundaries can be calculated using the same method, which will not be given in this paper for simplicity.

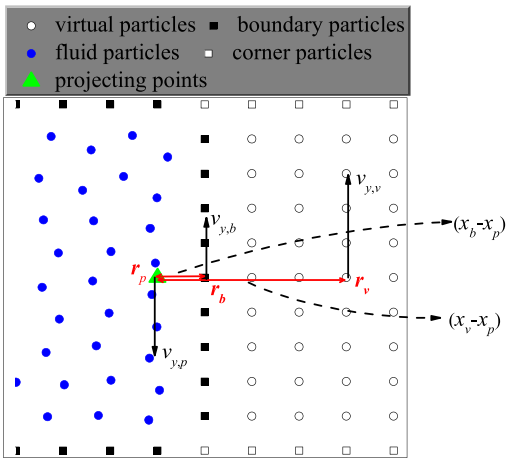

Figure 13. Schematic diagram of the calculation method of virtual particles flow variables.

DOI: 10.1002/fld

3. Corner particles. After calculating flow variables of all the virtual particles and boundary particles, the following equation is used to calculate the flow variables of corner particles:

$$f_c = \frac{\sum_j \frac{m_j}{\rho_j} f_j W_{cj}}{\sum_j \frac{m_j}{\rho_j} W_{cj}}, \tag{34}$$

where f_c represents the flow variables of corner particles. Eqns (34) and (30) have the same form, while the difference is that in Eq. (34), j represents all the particles including fluid particles, boundary particles, and virtual particles, as shown in Figure 14.

5.2. *Results and discussion*

Figure 15 shows the velocity distribution at $Re = 1$, using 50×50 particles based on the conventional SPH method, FPM, KGF-SPH, and the finite volume method (FVM). The FVM simulations are conducted with sufficient grid numbers, and therefore the results are regarded as convergent and accurate for comparison. As seen from Figure 15, the results of FPM and KGF-SPH are more close to the FVM than that of the SPH. The results of FPM and KGF-SPH are basically very close. While on the positions

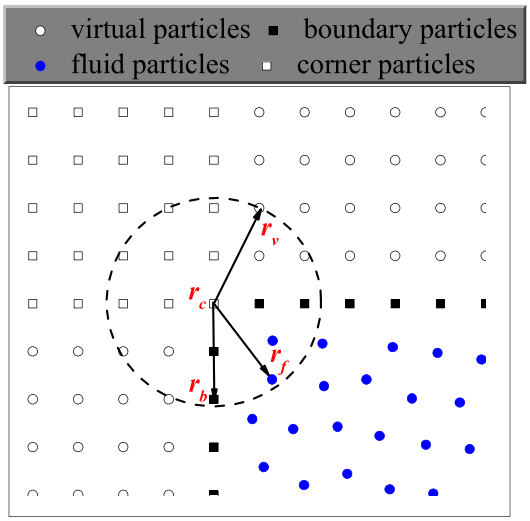

Figure 14. Particles interacting with the corner particles.

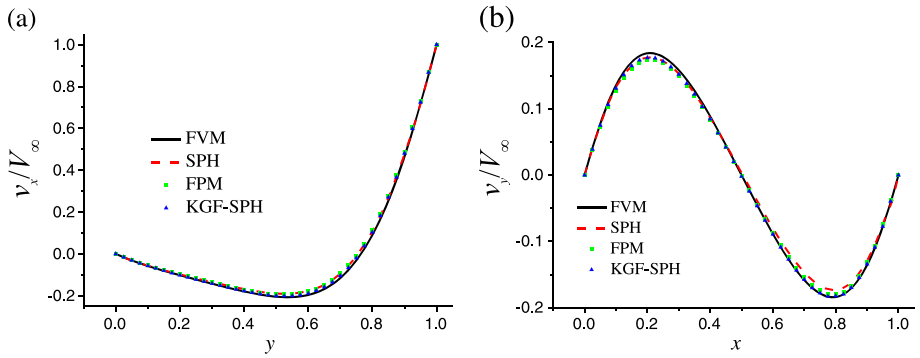

Figure 15. $Re = 1$, velocity profiles obtained by SPH, finite particle method (FPM), and kernel gradient free (KGF) SPH in lid-driven shear cavity at the steady state: (a) horizontal velocity profiles along the vertical centerline and (b) vertical velocity profiles along the horizontal centerline. FVM, finite volume method.

DOI: 10.1002/fld

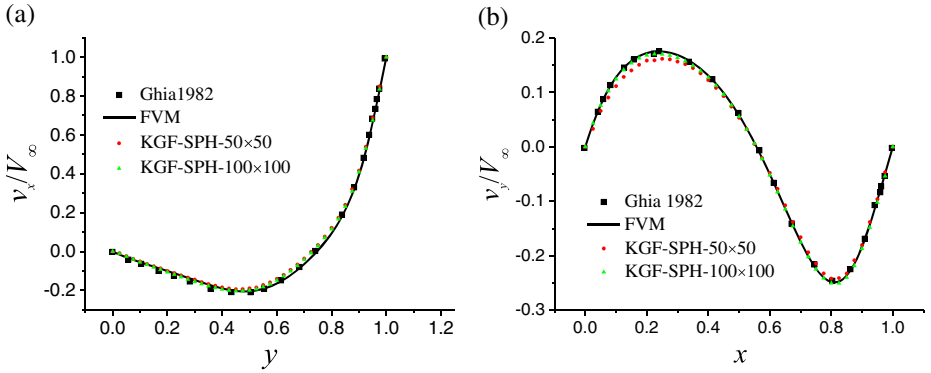

Figure 16. $Re = 100$, velocity profiles obtained by kernel gradient-free (KGF)-SPH in lid-driven shear cavity at the steady state: (a) horizontal velocity profiles along the vertical centerline and (b) vertical velocity profiles along the horizontal centerline. FVM, finite volume method.

where the velocity is largest (peak velocity) or smallest (valley velocity), the KGF-SPH is closer to the FVM solution than FPM. This reveals that KGF-SPH is more accurate than FPM and SPH.

Figure 16 shows the velocity profiles obtained by KGF-SPH and FVM, at $Re = 100$. The results of KGF-SPH were obtained by adopting 50×50 and 100×100 particles, respectively. As can be seen from Figure 16, when using 50×50 particles, results of KGF-SPH are very close to those from literature [32] and the FVM, but the minimum and maximum velocities have some discrepancies. When increasing particle number to 100×100, results from KGF-SPH simulation nearly coincide with the results from literature and FVM simulation. This further demonstrates that KGF-SPH is capable of getting convergent and accurate solutions.

6. CONCLUSIONS

In this paper, a KGF-SPH method is proposed. The KGF-SPH method is a modified FPM, which is a corrective SPH method with higher order accuracy. Similar to the original FPM, the KGF-SPH approximation is based on Taylor series analyses on a field function and its gradients. The difference is that in KGF-SPH, the kernel gradient in FPM is replaced by the kernel function multiplied by the particle spacing.

In summary, we can get following conclusions:

1. KGF-SPH retains all advantages of SPH (mesh-free, Lagrangian, and particle method) and shows the capability of treating free surfaces, moving interfaces, and large deformations.
2. As kernel gradients are not used in KGF-SPH, selection of smoothing kernel can be more flexible. Hence, kernels that are not differentiable or not sufficiently smooth can all be used in KGF-SPH simulation.
3. KGF-SPH is a corrective SPH method (similar to FPM) with higher order accuracy, and simulations using KGF-SPH should be insensitive to particle distribution. However, the corrective matrix from KGF-SPH is symmetric, and this is different from FPM in which the corrective matrix is asymmetric. It is clear that a symmetric matrix is much easier in mathematic processing than an asymmetric matrix. This is especially true in FPM when singular corrective matrix can usually happen.

To show the effectiveness and accuracy of KGF-SPH, numerical analyses are conducted for a number of polynomials. It is revealed that KGF-SPH is much more accurate than SPH and is capable of reproducing linear functions. It is also found that for higher order polynomials, KGF-SPH also has better accuracy than FPM, especially for simulations with bigger particle spacing. KGF-SPH is then applied to model a two-dimensional lid-driven shear cavity problem, which is an incompressible fluid flow and is usually used as a benchmark problem for novel CFD methods or algorithms. For different Reynolds number, KGF-SPH can get accurate results. It is also revealed that KGF-SPH is much more accurate than the conventional SPH and even than FPM with better peak and valley velocities.

DOI: 10.1002/fld

ACKNOWLEDGEMENTS

This work was supported by the National Natural Science Foundations of China (11172306) and (11372040).

REFERENCES

1. Liu MB, Liu GR, Lam KY. Constructing smoothing functions in smoothed particle hydrodynamics with applications. *Journal of Computational and Applied Mathematics* 2003; **155**:263–284.
2. Lucy LB. Numerical approach to testing of fission hypothesis. *Astronomical Journal* 1977; **82**:1013–1024.
3. Gingold RA, Monaghan JJ. Smoothed particle hydrodynamics: theory and application to non-spherical stars. *Monthly Notices of the Royal Astronomical Society* 1977; **181**:375–389.
4. Hu XY, Adams NA. An incompressible multi-phase SPH method. *Journal of Computational Physics* 2007; **227**:264–278.
5. Tartakovsky AM, Meakin P. A smoothed particle hydrodynamics model for miscible flow in three-dimensional fractures and the two-dimensional Rayleigh Taylor instability. *Journal of Computational Physics* 2005; **207**:610–624.
6. Tartakovsky AM, Tartakovsky DM, Scheibe TD, Meakin P. Hybrid simulations of reaction-diffusion systems in porous media. *Siam Journal on Scientific Computing* 2007; **30**:2799–2816.
7. Libersky LD, Petschek AG, Carney TC, Hipp JR, Allahdadi FA. High strain Lagrangian hydrodynamics: a three-dimensional SPH code for dynamic material response. *Journal of Computational Physics* 1993; **109**:67–75.
8. Randles PW, Libersky LD. Smoothed particle hydrodynamics: some recent improvements and applications. *Computer Methods in Applied Mechanics and Engineering* 1996; **139**:375–408.
9. Johnson GR, Beissel SR. Normalized smoothing functions for SPH impact computations. *International Journal for Numerical Methods in Engineering* 1996; **39**:2725–2741.
10. Liu MB, Liu GR, Lam KY. Adaptive smoothed particle hydrodynamics for high strain hydrodynamics with material strength. *Shock Waves* 2006; **15**:21–29.
11. Swegle JW, Attaway SW. On the feasibility of using smoothed particle hydrodynamics for underwater explosion calculations. *Computational Mechanics* 1995; **17**:151–168.
12. Liu MB, Liu GR, Lam KY, Zong Z. Smoothed particle hydrodynamics for numerical simulation of underwater explosion. *Computational Mechanics* 2003; **30**:106–118.
13. Liu MB, Liu GR, Zong Z, Lam KY. Computer simulation of high explosive explosion using smoothed particle hydrodynamics methodology. *Computers & Fluids* 2003; **32**:305–322.
14. Liu MB, Liu GR. Smoothed particle hydrodynamics (SPH): an overview and recent developments. *Archives of Computational Methods in Engineering* 2010; **17**:25–76.
15. Cleary PW, Prakash M, Ha J, Stokes N, Scott C. Smooth particle hydrodynamics: status and future potential. *Progress in Computational Fluid Dynamics* 2007; **7**:70–90.
16. Monaghan JJ. Smoothed particle hydrodynamics. *Reports on Progress in Physics* 2005; **68**:1703–1759.
17. Chen JK, Beraun JE. A generalized smoothed particle hydrodynamics method for nonlinear dynamic problems. *Computer Methods in Applied Mechanics and Engineering* 2000; **190**:225–239.
18. Chen JK, Beraun JE, Jih CJ. An improvement for tensile instability in smoothed particle hydrodynamics. *Computational Mechanics* 1999; **23**:279–287.
19. Chen JK, Beraun JE, Jih CJ. Completeness of corrective smoothed particle method for linear elastodynamics. *Computational Mechanics* 1999; **24**:273–285.
20. Liu MB, Liu GR. Restoring particle consistency in smoothed particle hydrodynamics. *Applied Numerical Mathematics* 2006; **56**:19–36.
21. Liu MB, Xie WP, Liu GR. Modeling incompressible flows using a finite particle method. *Applied Mathematical Modelling* 2005; **29**:1252–1270.
22. Batra RC, Zhang GM. Analysis of adiabatic shear bands in elasto-thermo-viscoplastic materials by modified smoothed-particle hydrodynamics (MSPH) method. *Journal of Computational Physics* 2004; **201**:172–190.
23. Fang JN, Owens RG, Tacher L, Parriaux A. A numerical study of the SPH method for simulating transient viscoelastic free surface flows. *Journal of Non-Newtonian Fluid Mechanics* 2006; **139**:68–84.
24. Chen JK, Beraun JE, Carney TC. A corrective smoothed particle method for boundary value problems in heat conduction. *International Journal for Numerical Methods in Engineering* 1999; **46**:231–252.
25. Monaghan JJ, Lattanzio JC. A refined particle method for astrophysical problems. *Astronomy and Astrophysics* 1985; **149**:135–143.
26. Morris JP, Fox PJ, Zhu Y. Modeling low Reynolds number incompressible flows using SPH. *Journal of Computational Physics* 1997; **136**:214–226.
27. Liu GR, Liu MB. *Smoothed Particle Hydrodynamics: A Meshfree Particle Method*. Singapore: World Scientific, 2003; 140–144.
28. Xu R, Stansby P, Laurence D. Accuracy and stability in incompressible SPH (ISPH) based on the projection method and a new approach. *Journal of Computational Physics* 2009; **228**:6703–6725.
29. Shadloo MS, Zainali A, Sadek SH, Yildiz M. Improved incompressible smoothed particle hydrodynamics method for simulating flow around bluff bodies. *Computer Methods in Applied Mechanics and Engineering* 2011; **200**:1008–1020.

DOI: 10.1002/fld

30. Takeda H, Miyama SM, Sekiya M. Numerical simulation of viscous flow by smoothed particle hydrodynamics. *Progress of Theoretical Physics* 1994; **92**:939–960.
31. Fabricio M, Antuono M, Gonzales LM, Colagrossi A. Theoretical analysis of the no-slip boundary condition enforcement in SPH methods. *Progress of Theoretical Physics* 2011; **125**:1091–1121.
32. Ghia U, Ghia KN, Shin CT. High-resolutions for incompressible flow using the Navier-Stokes equations and a multigrid method. *Journal of Computational Physics* 1982; **48**:387–411.

DOI: 10.1002/fld